Intelligence & Robotics

Research Article

Stability compensation of an admittance-controlled cartesian robot considering physical interaction with a human operator

Narawich Songthumjitti[1], Takeshi Inaba[2]

[1]Course of Electrical and Electronic Engineering, Graduate School of Tokai University, Kanagawa 259-1292, Japan.
[2]Department of Applied Computer Engineering, School of Information Science and Technology, Tokai University, Kanagawa 259-1292, Japan.

Correspondence to: Prof. Takeshi INABA, Department of Applied Computer Engineering, School of Information Science and Technology, Tokai University, Kanagawa 259-1292, Japan. E-mail: inaba@tokai.ac.jp

Abstract

In human-machine systems, admittance control is widely used for controlling robots. However, the problem with this method is that the stability can be impacted by the stiffness of the machine and the human operator. In order to minimize the oscillation issue that is caused by insufficient structure stiffness, this study used compensation methods, specifically feed-forward and acceleration feedback. Simulation results show that both compensation methods can expand the stability region of the system. Nevertheless, feedback compensation is more appropriate than feed-forward when taking into account uncertainties in the structure parameters of the system. Even when the system is not perfectly implemented, feedback compensation can keep the system stable, whereas feed-forward compensation causes a significantly reduced stability region. From the experiment, it is also confirmed that the feedback system has an advantage over the feed-forward system, and this simple feedback using an accelerometer can compensate for the insufficient stiffness of the robot structure and greatly enhance the stability of the human-machine system.

Keywords: Human-machine system, admittance model, system stability, compensator, feed-forward, feedback

1. INTRODUCTION

Robots are created to perform tasks more efficiently and accurately than human operators. In situations that are too dangerous or inaccessible for humans, deploying robots can provide a safer and more effective solution. However, in order to make a robot perform tasks, instructions must be given. While simple robot movements can be controlled with buttons, joysticks, or computer codes, tracing human movement while they perform difficult tasks is challenging. Another solution is to use a human–robot collaboration system, which enables direct interaction between human operators and robots [1–3]. In particular, power-assist systems and direct robot teaching are examples of applications for such systems in which human operators and robots physically interact [4]. In such systems, human operators will be able to guide the movements of a robot at will. To realize such systems, the robot must be properly controlled based on the manipulation force of the operator.

Admittance control is one method to realize such a system [5]. A human-machine system can be a closed-loop system consisting of an admittance-controlled robot and a human operator. Interaction forces are generated by end-effectors that are touched by humans, measured by force sensors, and input into the admittance model. However, admittance control has the disadvantage that the stability of the system is affected by the stiffness of the environment, the time delay of the control, and the bandwidth of the actuator [6,7]. In human-machine systems, the stiffness of the human and the stiffness of the structure of a robot are particularly important [8]. When human stiffness increases, to prevent robots from oscillating, the admittance model must be changed by increasing the viscosity and mass parameters [9]. Several variable admittance control methods have been proposed to improve operability [10], but the variable parameter range is limited to maintain stability [11–15]. If the structural characteristics of the original robot system have a large influence, the range of variable parameters will be narrow, and the improvement in operability will be limited. Especially in the case of cartesian robots, where the mass of the movable actuator is large, the force required to move that actuator itself is greater, so the effect of insufficient structural stiffness of the robot is greater. This requires a particularly large mass parameter in the admittance model to ensure stability, resulting in poor maneuverability.

In this study, we focused on improving the stability of the human-machine system without decreasing the admittance characteristic of the system. The idea is to make a compensator that can reduce the effect of structural characteristics that affect system stability to a minimum. Buerger et al. propose a method for designing an actuator controller for an interactive robot with structural resonance [16]. This approach is similar to ours, as it uses a feedback controller to compensate for the structural characteristics of the robot and shape the open-loop characteristics to improve stability. However, it assumes force control of the actuator and is difficult to incorporate into admittance control, which is position-based impedance control. Therefore, we propose a new method to compensate for the structural characteristics of the robot that can be easily applied to admittance control.

To design a compensator for use in the system, we have to know the characteristics of the robot, which consist of an actuator system and structural characteristics, which can be obtained through a spectrum analysis experiment [17]. After that, a compensator can be designed to achieve a wider stability range in operation. Therefore, we can use lower inertia and viscosity parameters in the admittance model, which means the operator can work in a lighter environment and extend the operation duration before starting to get tired. We consider feed-forward and feedback compensators. Feed-forward compensators are simple and require no extra sensors, but they are not robust to changes in the structure characteristics. In contrast, feedback compensators are robust but require sensors to measure the motion of the structure. Motion sensors on actuators (typically rotary encoders, etc.) are relatively internal sensors and cannot measure absolute motion, which is important for interaction with the operator outside the robot. In this study, the absolute motion of the structure is measured by accelerometers that can be easily attached to the structure of the robot.

The results from simulations show that by appending feed-forward and feedback compensation, they can ex-
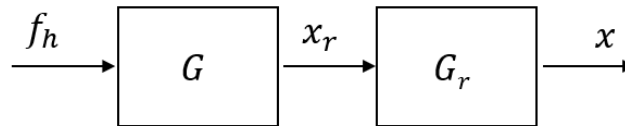
Figure 1. Block diagram of an admittance control robot, where G represents the admittance model, and G_r represents the robot characteristic transfer function.

pand the stability region by a significant amount. However, the stability region of a feed-forward compensated system will easily decrease if the structure characteristic of the actual system is not the same as the measurement. Therefore, we designed a feedback compensated system to overcome this limitation. With feedback compensation, the system can maintain the stability region even if the structure characteristics change from our measurement.

Experiments are carried out to test the improvement of the compensated systems. The results show that both systems can stably operate with a higher admittance characteristic, indicated by a lower mass parameter, compared to the uncompensated system. And also, feedback compensation can operate at a lower mass parameter in the admittance model compared to feed-forward compensation, which means feedback compensation is more robust and preferable in practical application.

2. ADMITTANCE CONTROL OF THE HUMAN-INTERACTIVE ROBOT

2.1. Admittance control
The admittance control is a way to control robots with human interaction; control input to the system will come from the applied force of human operators, and the robot will move according to the admittance model to the desired position. Admittance is the inverse of impedance, and an impedance model is a transfer function that receives position information and calculates force output; therefore, an admittance model will receive force input information, f_h, and calculate position information, x_r. In combination with a position-controlled robot, as shown in Figure 1, where G represents the admittance model, and G_r represents the robot characteristic transfer function. The calculated position reference, x_r, can be directly fed into the system, and the robot position, x, will move to the desired position.

We consider the mass spring damper system as an admittance model. However, in our study, it does not need to return to the origin after the operator breaks the contact, so the stiffness parameter can be neglected. The transfer function of the admittance model, G, will be represented as Equation (1). Lowering the coefficient results in a lighter workload for the operator and less stability in the system. On the other hand, a higher coefficient increases the workload for the human operator in exchange for greater system stability.

$$G = \frac{1}{Ms^2 + Ds} \tag{1}$$

2.2. Human-machine system
The robot requires instructions to move according to the needs of the human operator. The admittance control method is used when control is input via human-robot interaction. As shown in Figure 2, a robot that makes contact with the operator forms a single-couple system, and human interaction creates a closed-loop system[5]. The impedance of the human operator, H, will create force, f_h, according to errors that come from the displacement of the robot, x, subtracted from the intended position of the operator, x_d. The force that a human operator needs to apply to the system is highly dependent on the admittance characteristics of the
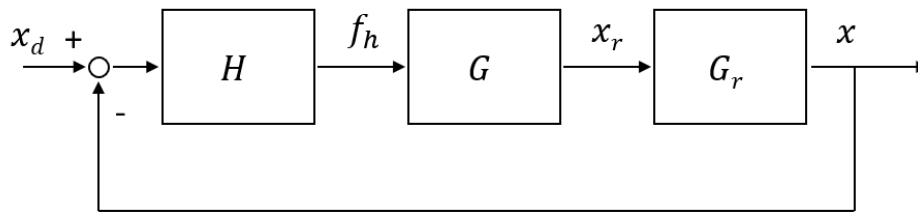
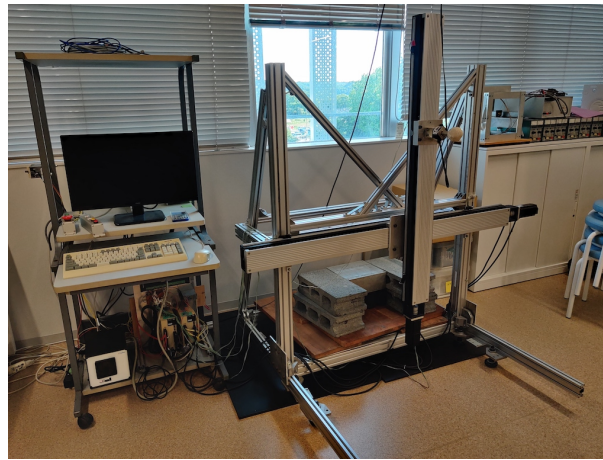**Figure 2.** Human-machine interaction diagram.

Figure 3. Experiment setup.

system.

Closed-loop systems can have instability problems that also depend on G_r, which represents the transfer function of the robot. System instability will occur if it is not optimally implemented, particularly because the dead time that exists in every system will cause a system delay in responding to commands and insufficient stiffness of the structure, resulting in oscillation if the admittance model is not low enough. However, if the admittance model is too low, it will affect maneuverability. So, we will derive the model of the experiment system that takes into account these properties mentioned above. Furthermore, we also consider a compensator for implementation in the system.

3. MODELING

3.1. Experiment setup

The experiment setup shown in Figure 3 is designed for a power-assisted robot system. It is equipped with a force sensor, AC servo motors, servo packs, and linear sliders. A laser distance sensor is used for only spectrum analysis, and an acceleration sensor is used for feedback compensation mentioned later. These devices are connected to a PC, as shown in Figure 4, to form the experiment setup, where the PC performs measurements, calculates control operations, and outputs position command pulses to the servo packs with a sampling time of 1 ms.
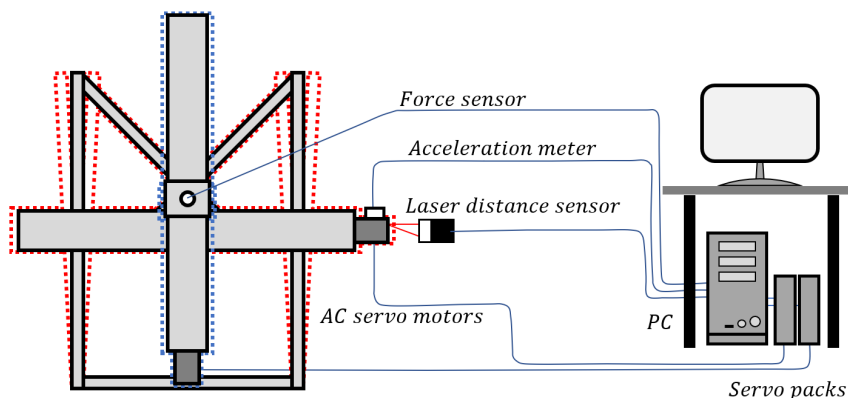
Figure 4. Experiment setup diagram.

Table 1. Force sensor specification

Force sensor	
Manufacture	Nitta
Model	IFS-50M31A25-I25
Rated Input Force (XY)	100 N
Rated Input Force (Z)	200 N
Rated Input Torque (XYZ)	5 Nm

Table 2. Servo packs specification

Servo packs	
Manufacture	Yaskawa Electric Corporation
Model	SGDV-2R8F01A

Table 3. AC servo motors specification

AC servo motors	
Manufacture	Yaskawa Electric Corporation
Model	SGMJV-04ADA2C
Rated Output	400 W
Rated Torque	1.27 Nm
Rated Current	2.7 Arms
Rated Rotational Speed	3000 rpm
Encoder	20-bit serial encoder (incremental)

3.1.1. Force sensor

A Force sensor is a device used to measure the applied force and sends out digital data to the computer. In this experiment, the force/torque sensor from Nitta was used, and its specifications are shown in Table 1.

3.1.2. Servo packs & AC servo motors

Servo packs and AC servo motors are devices that work together. Servo packs supply electrical power to an AC servo motor, and the motor feeds feedback data from an encoder attached to its end to the servo pack, which detects the current position and adjusts the electrical power so that the AC servo motors turn to the correct position. Tables 2 and 3 show the specifications of the servo packs and AC servo motors used in the experiment.

3.1.3. Linear sliders

The servo motor creates rotational motion, but in this experiment, the robot needs to move in horizontal and vertical linear motion; therefore, linear sliders are used to convert rotational motion to linear motion. The

Table 4. Horizontal axis linear slider specification

Horizontal axis linear slider	
Manufacture	NSK
Model	MCH10105H20D
Nominal Stroke	1050 mm
Ball Screw Lead	20 mm
Mass	33 kg

Table 5. Vertical axis linear slider specification

Vertical axis linear slider	
Manufacture	NSK
Model	MCH10100H20K
Nominal Stroke	1110 mm
Ball Screw Lead	20 mm
Mass	27 kg

Table 6. Laser distance sensor specification

Laser distance sensor	
Manufacture	Panasonic
Model	HG-C1030
Output Type	NPN output
Measurement Center Distance	30 mm
Measurement Range	±5 mm

Table 7. Acceleration sensor specification

Acceleration sensor	
Manufacture	Kionix
Model	KXR94-2050
Measurement Range	±2G
Sensitivity	660mV/G
Frequency Range	800Hz (-3dB)

specification of the horizontal axis linear slider is shown in Table 4, and the specification of the vertical axis linear slider is shown in Table 5.

3.1.4. Laser distance sensor
For spectrum analysis, structure displacement must be measured. Therefore, a laser distance sensor is placed in the system to be used to measure structure displacement that results from oscillation, and its specifications can be found in Table 6.

3.1.5. Acceleration sensor
In subsequent sections, we use the acceleration of the structure of the robot as feedback to the control system, so an acceleration sensor is attached to the frame. Its specifications are listed in Table 7.

3.2. Modeling
3.2.1. Actuator system transfer function
The actuator system is required to move the robot to the desired coordinate. It consists of servo packs, AC servo motors, and linear sliders, where each component has its own characteristics. In this study, we will represent the characteristic of all these components with one transfer function, G_a, which consists of a second-order low-pass filter and a time delay, which come from an experiment and will be further explained in the section on spectrum analysis. To facilitate stability analysis, the time delay from the transfer function Equation (2) is approximated using the Pade approximation method.
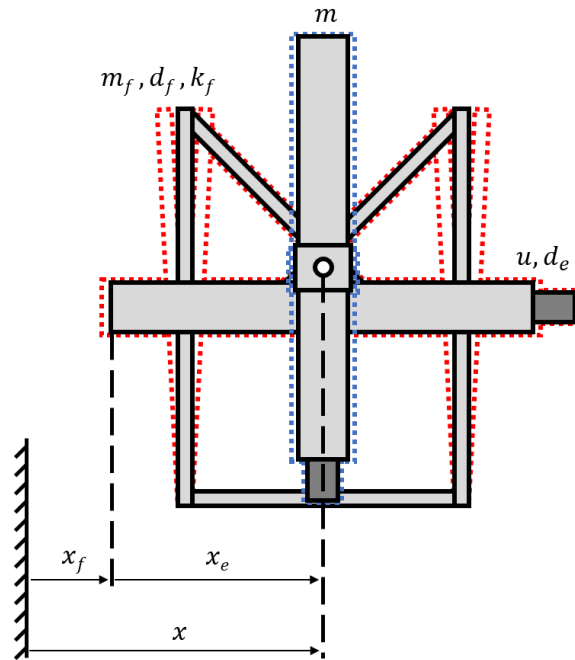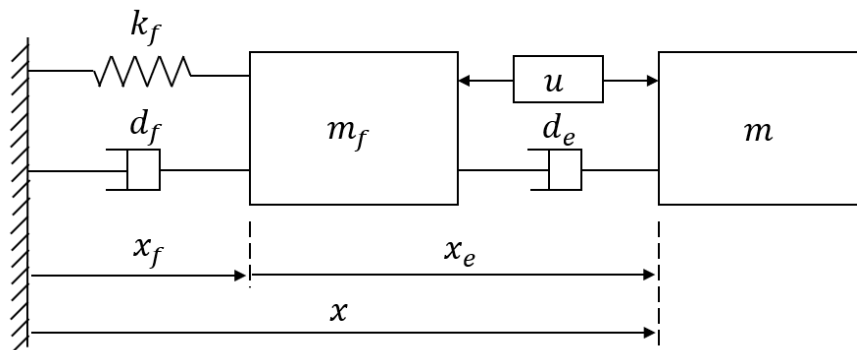
Figure 5. Structure model parameter.

Figure 6. Diagram of a simplified structure model.

$$G_a = \frac{\omega_a^2}{s^2 + 2\zeta_a\omega_a s + \omega_a^2} e^{-L_a s} \tag{2}$$

3.2.2. Structure transfer function

From the test bench shown in Figure 3, a structure has an X- and Y-axis actuator in the system, as shown in Figure 5. From our previous research, we found that the X-axis is more unstable compared to the Y-axis when a human operator interacts with the robot. So, in this study, we will concentrate on only the X-axis, which leads to system instability. We consider the horizontal structure movement as a single mass spring damper system in which the parameters are m_f, k_f, and d_f. For the X-axis actuator, the actuation force is displayed as u, and the viscosity of the actuator is displayed as d_e. It applies force to the Y-axis actuator and the frame. The mass of the Y-axis actuator is displayed as m. A simplified model is shown in Figure 6. Therefore, the transfer function can be derived using the free-body diagram as follows:

Absolute displacement of the robot end-effector, x, is the sum of absolute structure displacement, x_f, due to structure flexibility and relative displacement, x_e, from the actuator movement.

Equations (3 and 4) are created by focusing on all forces applied to each mass; therefore, derived equations will get a transfer function, as shown in Equation (5).

$$m_f \ddot{x}_f = -d_f \ddot{x}_f - k_f x_f - u + d\dot{x}_e \tag{3}$$

$$m\ddot{x} = u - d\dot{x}_e \tag{4}$$

$$G_s = \frac{X_f}{X_e} = \frac{-ms^2}{(m_f + m)s^2 + d_f s + k_f} \tag{5}$$

3.3. Spectrum analysis

Spectrum analysis is the process of analyzing a signal in the frequency domain, which reveals the frequencies and their associated magnitudes and phases that are present in the signal. This can be used to identify frequency components within a signal. In this study, Spectrum analysis is used for creating a Bode diagram of a system using input and output signals that are measured from the test system.

The fast Fourier transform algorithm is a widely used method for spectrum analysis that can calculate the discrete Fourier transform of a given signal. However, this algorithm is unsuitable for analyzing noise signals that are random and stochastic because it does not have well-defined frequencies. To analyze noise signals, power spectral analysis is a more suitable method. It can estimate the power of a signal at each frequency. But this method is still for analyzing a single signal. A cross-power spectral density, an extension of power spectral analysis, can give the result of total noise power spectral density in complex values at each frequency and is used to analyze the correlation between two signals.

The cross-correlation method is used to find the amplitude and frequency relationship between two signals. It can be expressed as Equation (6), where E is the expected value. For finite discrete-time signals, it can be mathematically expressed as Equation (7), where N is the length of the signals $x(n)$ and $y(n)$, and k ranges from $-(N-1)$ to $(N-1)$.

$$R_{xy}(k) = E[x(n)y(n+k)] \tag{6}$$

$$R_{xy}(k) = \sum_{n=0}^{N-1} x(n)y(n+k) \tag{7}$$

The cross-power spectral density is the Fourier transformation of cross-correlation as Equation (8). For finite discrete-time signals, it can be mathematically expressed as Equation (9). In this study, the `cpsd` function in MATLAB was used to calculate the cross-power spectral density.

$$S_{xy}(\omega) = \mathcal{F}[R_{xy}(k)] \tag{8}$$

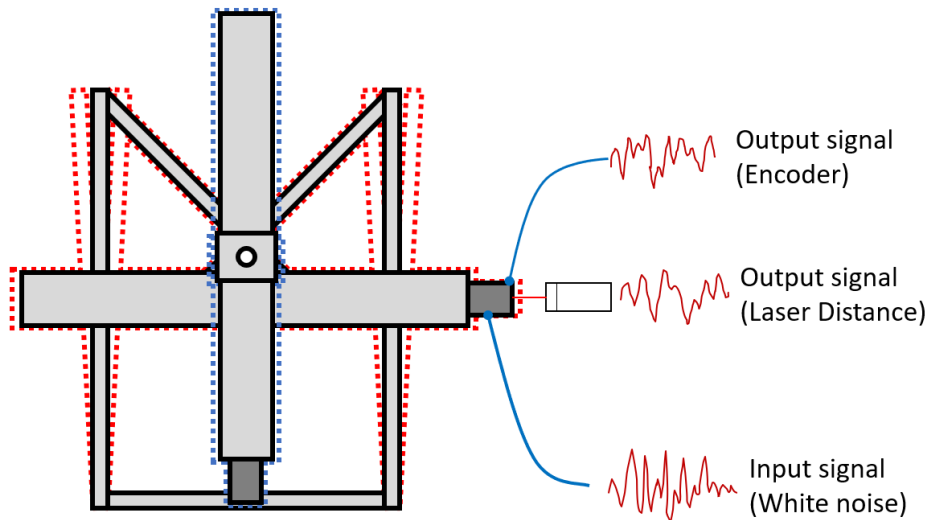$$S_{xy}(\omega_k) = \sum_{k=-(N-1)}^{N-1} R_{xy}(k)e^{-j\omega_k} \tag{9}$$

Figure 7. Spectrum analysis experiment setup.

The transfer function can be estimated using the cross-power spectral density of the input and output signals, as shown in Equation (10), and the magnitude and angle of the complex number results will yield the transfer function amplitude and phase.

$$G(j\omega_k) = \frac{S_{xy}(\omega_k)}{S_{xx}(\omega_k)} \qquad (10)$$

In this experiment, white noise is generated and used as the input of the system. and the output of the system consists of actuator displacement from the rotary encoder attached to the servo motor and structure displacement from the laser distance sensor, as shown in Figure 7. This data will be used to determine the actuator system and structure characteristics.

Actuator displacement, x_e, is regarded as an input to the structure transfer function, G_s, with frame displacement, x_f, as an output. Therefore, by fitting a curve using the Bode diagram shown in Figures 8 and 9, the characteristic parameter of a structure can be obtained.
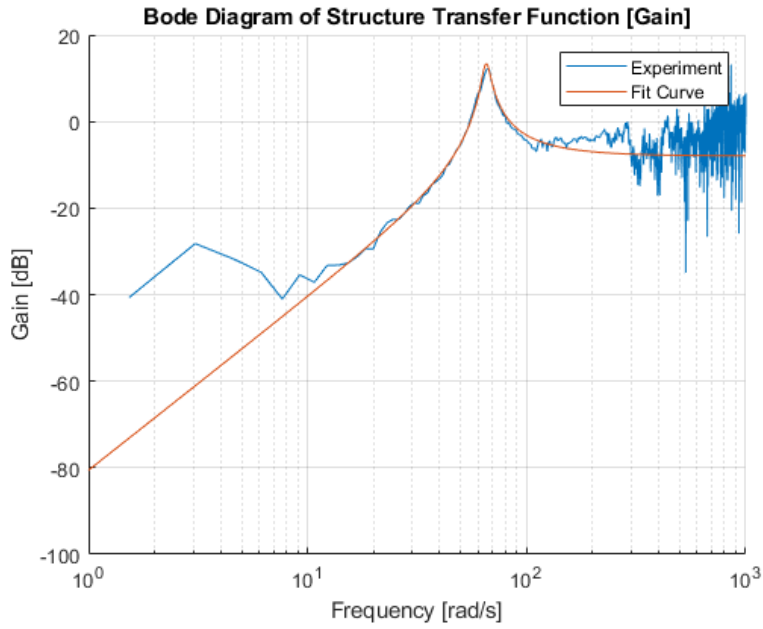
Bode Diagram of Structure Transfer Function [Gain]

Figure 8. Bode diagram of structure.

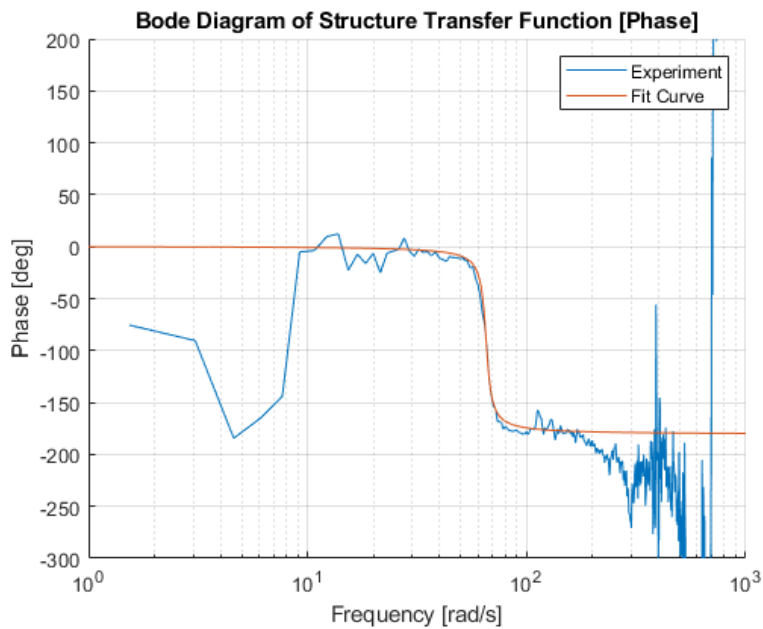**Bode Diagram of Structure Transfer Function [Phase]**

Figure 9. Phase diagram of structure.

The actuator system receives control system signal input, x_r, and output displacement, x_e. From the result, we can obtain parameters in the actuator system transfer function, G_a, by a fit graph of spectrum analysis, as shown in Figures 10 and 11. And we also use the Pade approximation to represent the time delay in the transfer function.

Resulting constants were $\omega_a = 75$ rad/s, $\zeta_a = 0.707$, $L_a = 3.5$ ms, $m_f = 45$ kg, $m = 30$ kg, $d_f = 420$ Ns/m, and $k_f = 320000$ N/m, respectively.
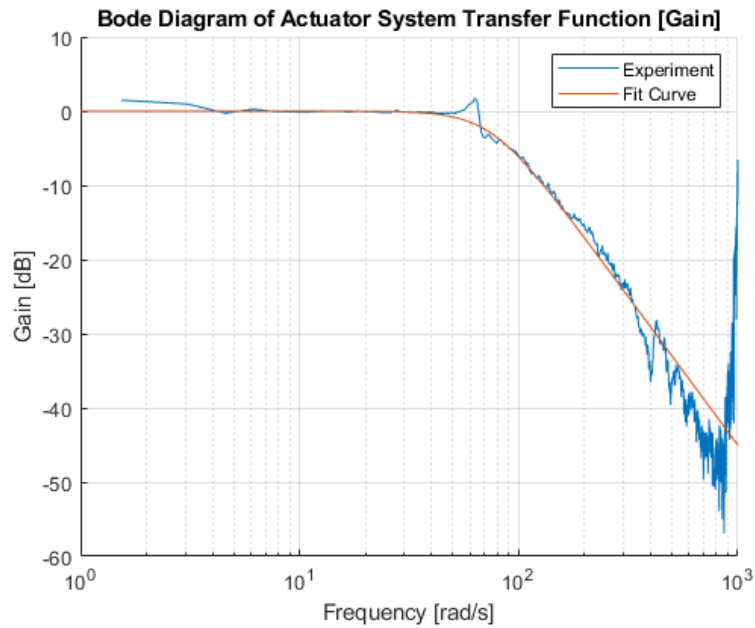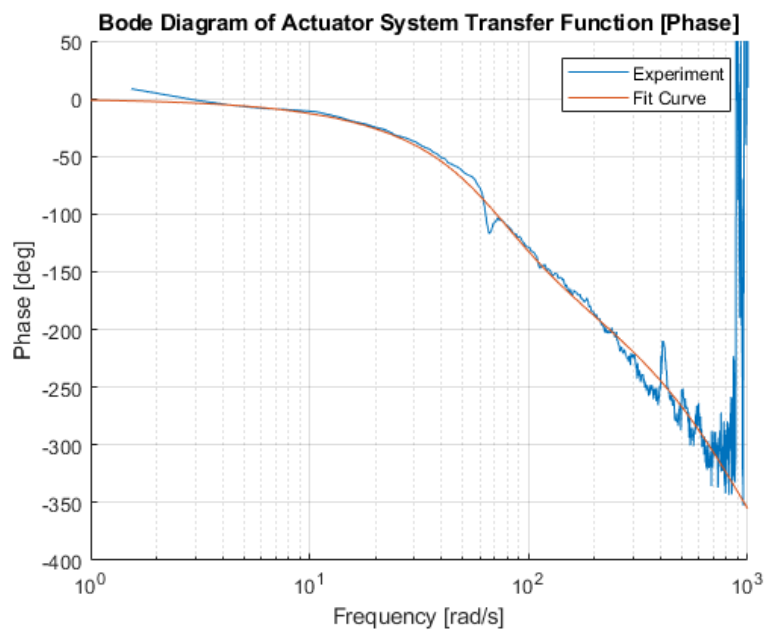
Figure 10. Gain diagram of an actuator system.

Figure 11. Phase diagram of an actuator system.

4. STABILITY ANALYSIS

4.1. Block diagram and transfer function of human-machine system

To analyze the stability of the experiment system, including the human operator, we need to consider the block diagram, as shown in FFigure 12. The human operator impedance, H, will react to errors that result from the absolute end-effector position, x, subtract from the operator-hand intended position, x_d, and create force, f_h, for the admittance model, where hand impedance is used for modeling human operators as in Equation (11). Each parameter will change according to the controlled object and posture of the operator[18,19].
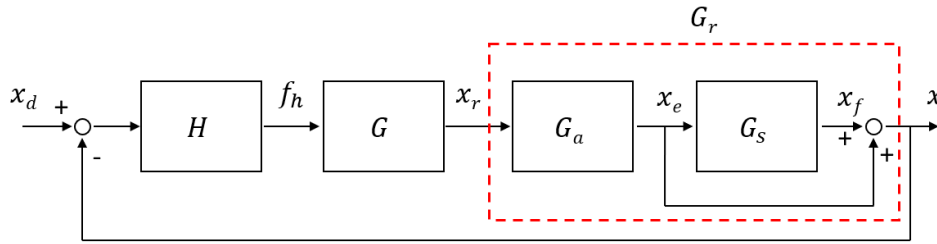
Figure 12. Experiment setup block diagram.

$$H = m_h s^2 + d_h s + k_h \tag{11}$$

Due to the insufficient stiffness of the robot, structure displacement that is created by robot movement has to be considered, so the absolute end-effector position, x, will consist of a summation of the relative actuator displacement, x_e, and the absolute structure displacement, x_f. Therefore, the position-control robot transfer function, G_r, consists of the linear actuator system transfer function, G_a, and the structure transfer function, G_s.

As a result, we can express the overall transfer function, G_{sys}, from the intended position of the operator, x_d, to the end-effector position, x, with Equation (12).

$$G_{sys} = \frac{HGG_a(G_s + 1)}{HGG_a(G_s + 1) + 1} \tag{12}$$

4.2. Stability margin

Phase margin is a method used to check the stability of the feedback system. It measures how much phase shift can be applied before the system becomes unstable. To check the stability of a feedback system, we have to determine the open loop transfer function of the system and then find the gain crossover frequency, which is the point where the gain is unity. If the phase at that point is greater than $-180°$, the system is considered stable, and more phase margin means a more stable system. The system transfer function is expressed as Equation (12), and the phase margin can be calculated from the open-loop transfer function $HGG_a(G_s + 1)$.

When the system is in contact with a human operator, it might become unstable. The harder the operator grabs the end-effector, the more the system will oscillate, and the impedance of the operator, H, is greatly affected by grip strength. Therefore, in stability analysis, the stiffness of the impedance of the operator, k_h, is a major component to be considered for stability.

In this section, we simulated system stability with changes in M and D in the admittance model to see how they affected overall system stability. The human impedance constants are $m_h = 1$ kg and $d_h = 17$ Ns/m, respectively, and k_h varies between $1 - 10000$ N/m, based on our previous study[18,19]. The simulation in Figures 13-15 is performed by fixing the mass parameter in the admittance model, M, and varying the damping coefficient in the admittance model, D, from $0.1 - 1000$ Ns/m. Figures 16-18, on the other hand, will be simulated by fixing the damping coefficient constant and varying the mass parameter from $0.1 - 1000$ kg.
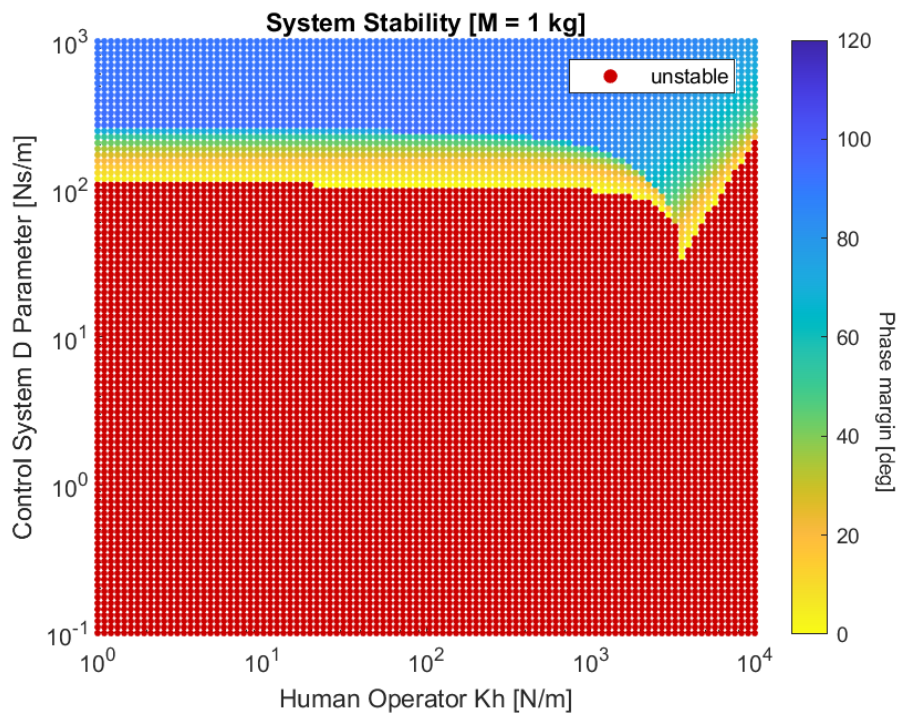
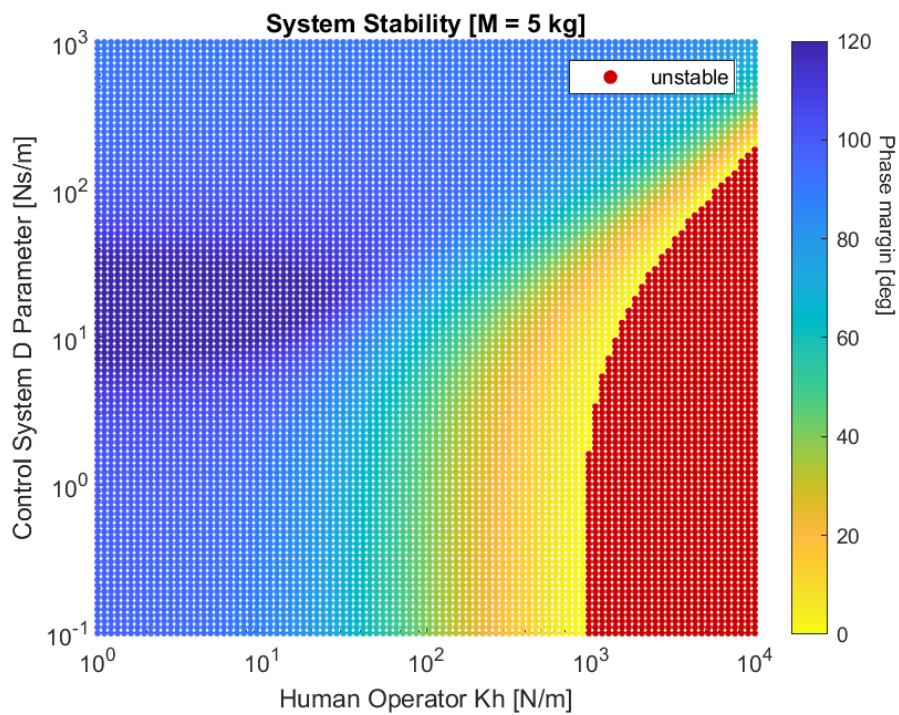**Figure 13.** Stability analysis with mass parameter, M, at 1 kg.

Figure 14. Stability analysis with mass parameter, M, at 5 kg.
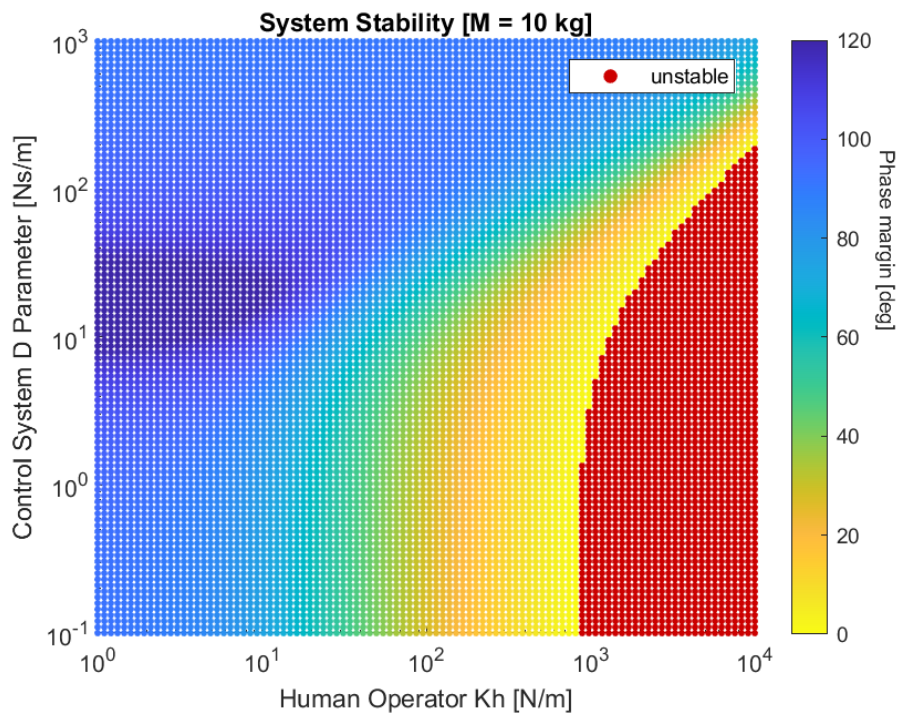
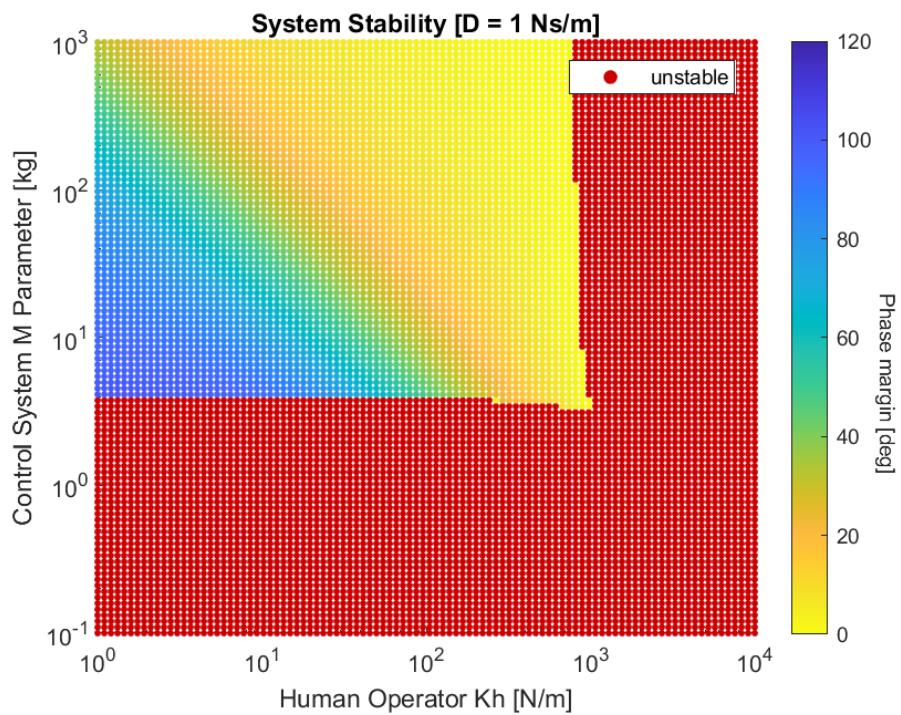**Figure 15.** Stability analysis with mass parameter, M, at 10 kg.

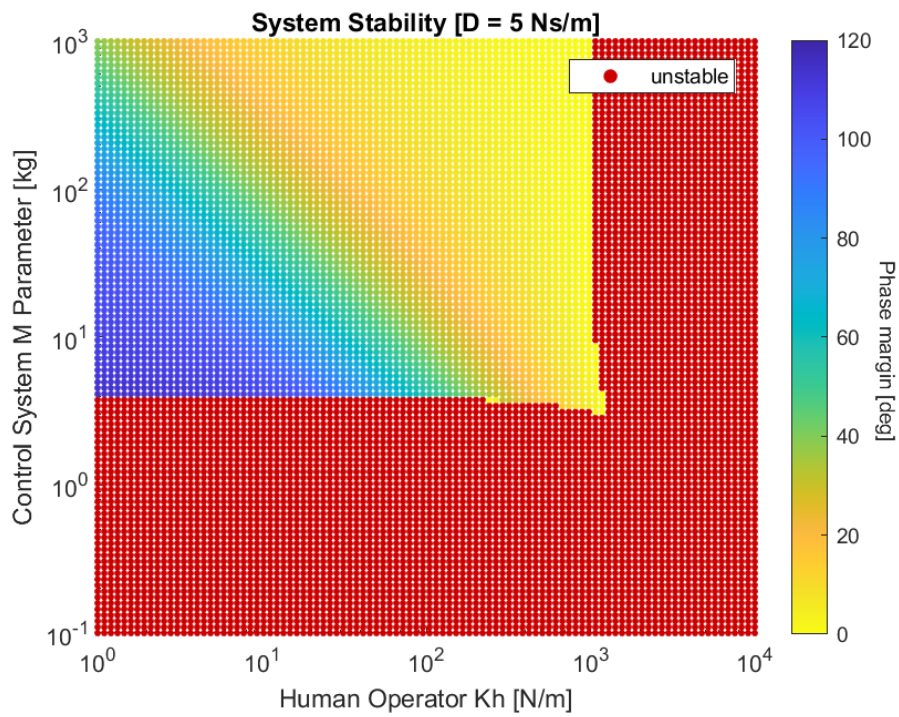**Figure 16.** Stability analysis with damping coefficient, D, at 1 Ns/m.

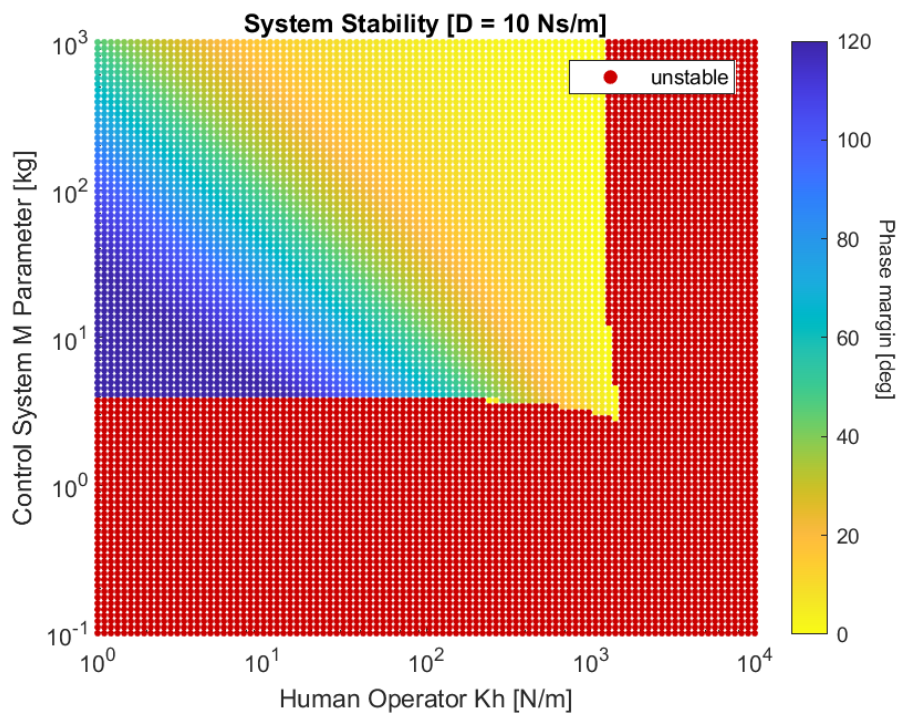**Figure 17.** Stability analysis with damping coefficient, D, at $5\,\text{Ns/m}$.

Figure 18. Stability analysis with damping coefficient, D, at $10\,\text{Ns/m}$.
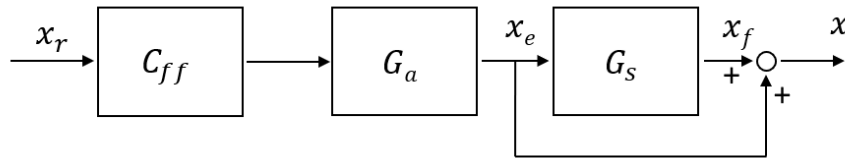
Figure 19. Feed-forward system block diagram.

According to the results in Figure 13, the system is unstable until the damping coefficient exceeds around $100\,\mathrm{Ns/m}$. Figures 14 and 15 show that changes in the damping coefficient around $0.1 - 20\,\mathrm{Ns/m}$ have little effect on the stability region of the system. Although the damping coefficient has a significant impact on system stability when its value exceeds $20\,\mathrm{Ns/m}$, in the human-machine system admittance model, G, must remain high for light operation, so this parameter must be small. Therefore, we can consider that the damping coefficient has no effect on the stability region in this study.

Moving on to Figures 16-18, it is shown that changing the value of the damping parameter, D, in the admittance model may not change much in the stability region. In a stable region, the mass parameter, M, greatly affects the phase margin. In conclusion, the results from the simulation show that changing the mass parameter will have a significant effect on system stability compared to changing the damping coefficient, which has little effect. So, in later simulations, we will only concentrate on changes in the mass parameter.

Figures 16-18 also show that to maintain system stability, the stiffness of the human operator, k_h, must not exceed about $1000\,\mathrm{N/m}$, and the mass parameter of the admittance model should be greater than around $5\,\mathrm{kg}$. Because of insufficient structure stiffness and dead time in the actuation system, the stability region is decreasing from the ideal system. This restriction in stiffness of the human operator, k_h, is allowable, but for the mass parameter, M, it is too large for a human to operate comfortably. Therefore, we should consider adding a compensator to the system that will expand the stability region.

5. FEED-FORWARD COMPENSATION

5.1. Design

A feed-forward compensator is a control system component that is used to improve the performance of the system. As shown in Figure 19, the compensator is inserted in series with the control system. In this study, we tried to minimize the effect of structure characteristics by adding a simple compensator to the system. The compensator, C_{ff}, as shown in Equation (13), consists of an inverted transfer function from relative actuator displacement, x_e, to absolute end-effector displacement, x, but we do not include the actuator transfer function, G_a, in the compensator because of its unstable zero that comes from the Pade approximation of dead time. The idea of this compensator is to cancel out the characteristics of the structure that cause the system to become unstable in some conditions. Therefore, the overall transfer function includes the compensator of the feed-forward compensated system, G_{xxr}, which can be expressed as Equation (14).

$$C_{ff} = \frac{1}{G_s + 1} \tag{13}$$

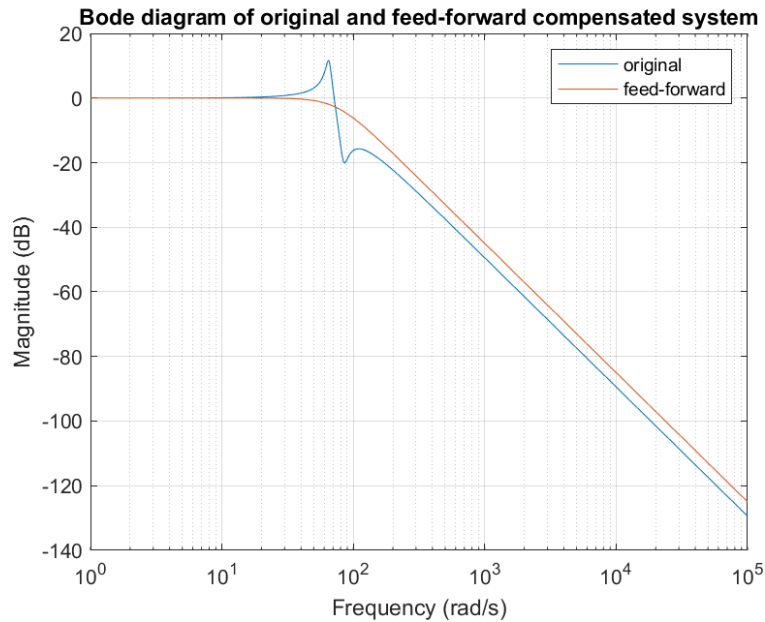$$G_{xxr} = \frac{x}{x_r} = G_a \tag{14}$$

Figure 20. Bode diagram of the original and feed-forward compensated system.

In Figure 20, the Bode diagram shows the response of the overall robot transfer function, G_{xxr}, of the original system and feed-forward compensated system. In the original system, it has an effect from the structure characteristics at around 70 rad/s that can cause an oscillation when a human is in contact with it. And after we append a feed-forward compensator, it shows that it can cancel out the effect of the structure characteristics.

5.2. Simulation

The compensator that is applied to the system is the inverse of the structure transfer function, so we have to consider the error of the structure parameter measurement because if the measurement is not exactly the same as the actual system, the designed compensator will not cancel out the structure transfer function. With this situation, we also need to consider that the actual system has a different natural frequency from the measurement, and the parameter that directly changes natural frequency is the stiffness of the structure and the mass of the structure. In this simulation, we consider the change in structure stiffness, k_f. So, in this simulation, we use parameter $D = 1$ Ns/m in the admittance model, and we tried to simulate stability with an actual system that has the exact same stiffness as the measurement, as shown in Figure 21, the simulation with an actual system that has stiffness 20% less than the measurement, as shown in Figure 22, and the simulation with an actual system that has stiffness 20% greater than the measurement, as shown in Figure 23.
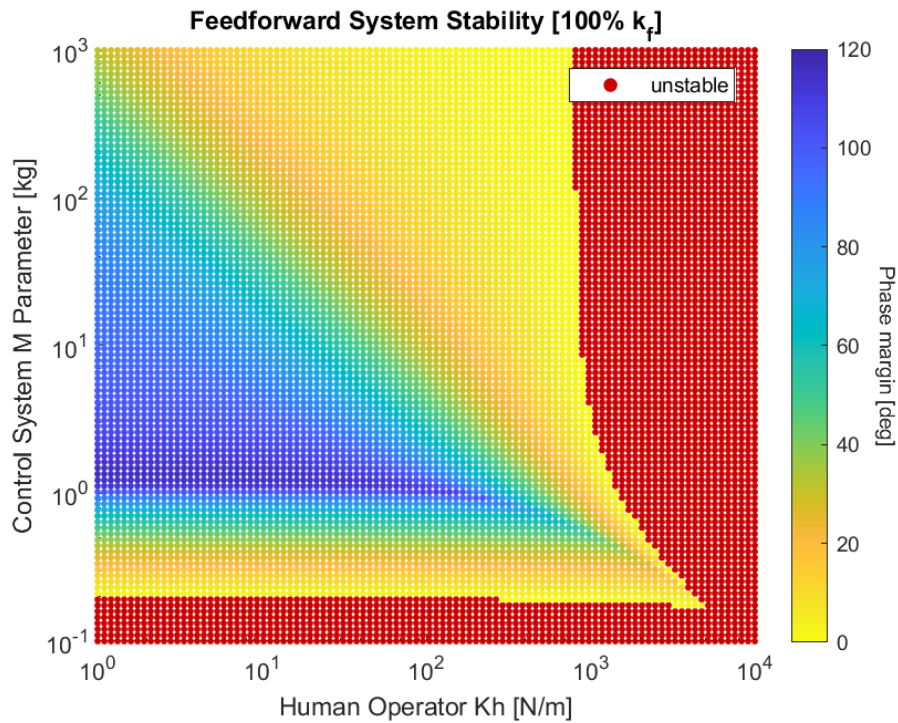
Figure 21. Feed-forward system stability analysis with actual system structure stiffness at 100%.
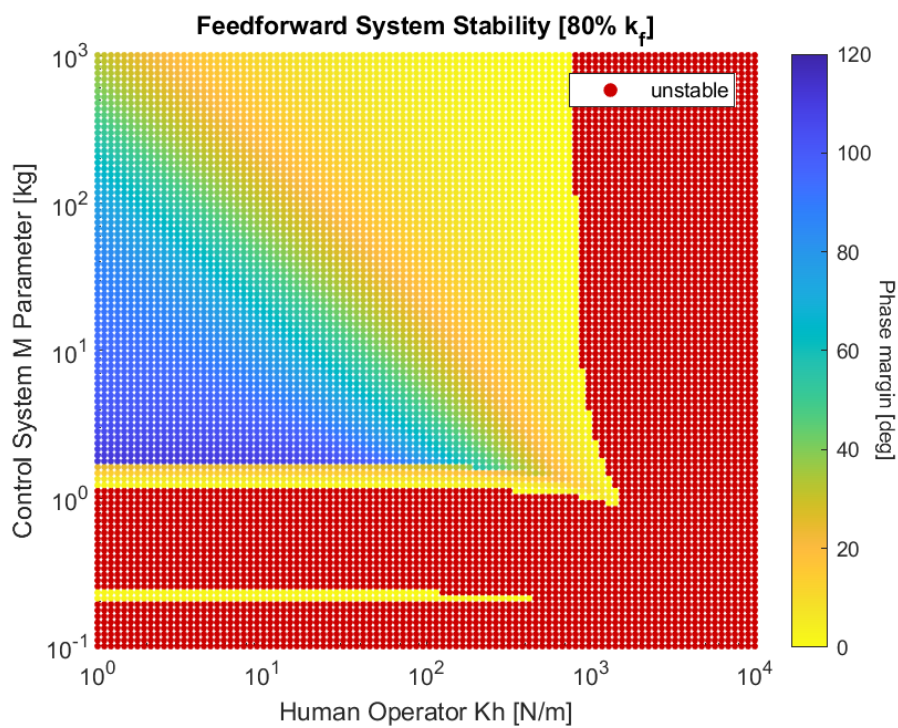
Figure 22. Feed-forward system stability analysis with actual system structure stiffness at 80%.

From Figure 21, when the compensator perfectly cancels out the structure characteristic, the stability region is increased compared to the system without compensation shown in Figure 16. It shows that a feed-forward
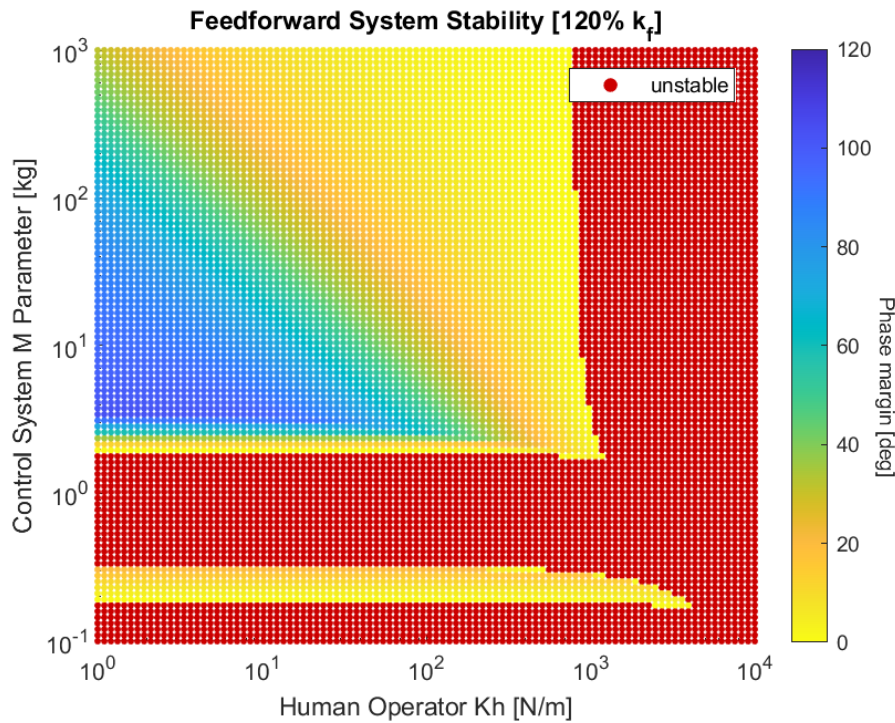
Figure 23. Feed-forward system stability analysis with actual system structure stiffness at 120%.

compensator allows us to use a smaller M parameter in the admittance model to around $0.2\,\text{kg}$, which is an improvement from a non-compensated system that can use $M = 5\,\text{kg}$ or above. However, when the actual system parameter is not the same as the measurement, it causes a reduction in the stability region. As shown in Figures 22,23, the allowable M parameter in the admittance model is around 1 and $1.5\,\text{kg}$, respectively, which is much greater than the perfectly compensated system, as shown in Figure 21.

To easily compare the stability region between an uncompensated and a feed-forward system, we display the stability boundary of both simulations in the same graph, as shown in Figure 24 for a perfectly compensated system and Figure 25 for a system considered to have a +20% stiffness parameter measurement error. These two figures show that errors in stiffness parameters greatly affect the stability region of a feed-forward compensated system. Although in Figure 25, the stability region of a feed-forward system is reduced, it still has an advantage over the system without compensation.
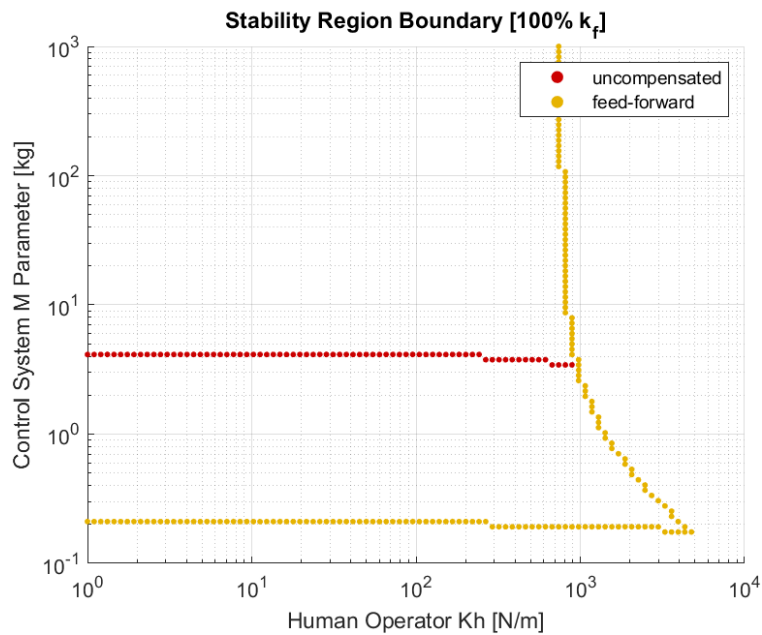
Stability Region Boundary [100% k$_f$]

Figure 24. Stability region boundary comparison between a non-compensated system and a feed-forward system at 100% k_f.
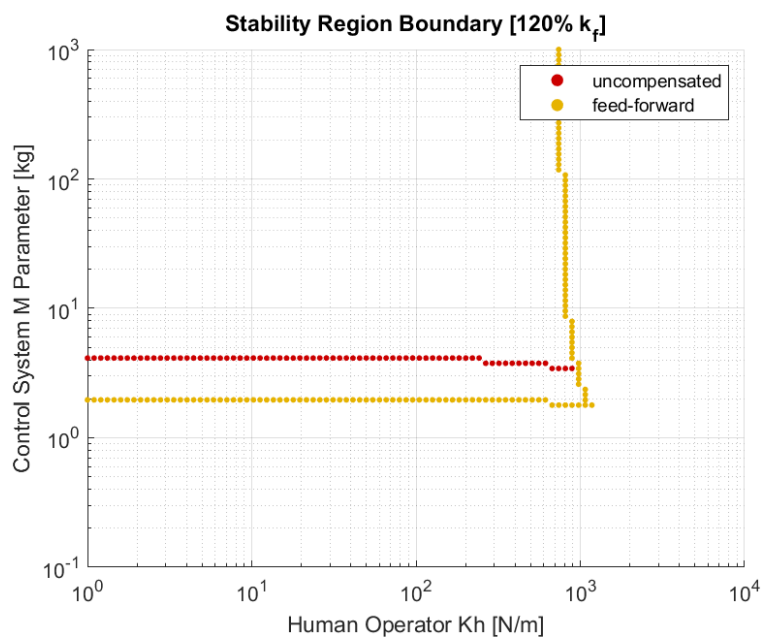
Stability Region Boundary [120% k$_f$]

Figure 25. Stability region boundary comparison between a non-compensated system and a feed-forward system at 120% k_f.

5.3. Experiment

In this experiment, we use the admittance model parameter as follows: $M = 2\,\text{kg}$, $D = 1\,\text{Ns/m}$, because with these values, a non-compensated system will be in an unstable region, but a system with a feed-forward compensator will be in a stable region even though we take stiffness parameter measurement errors into account, as shown in Figure 25, which we can use to check whether the stability region is improving according to the simulation or not.
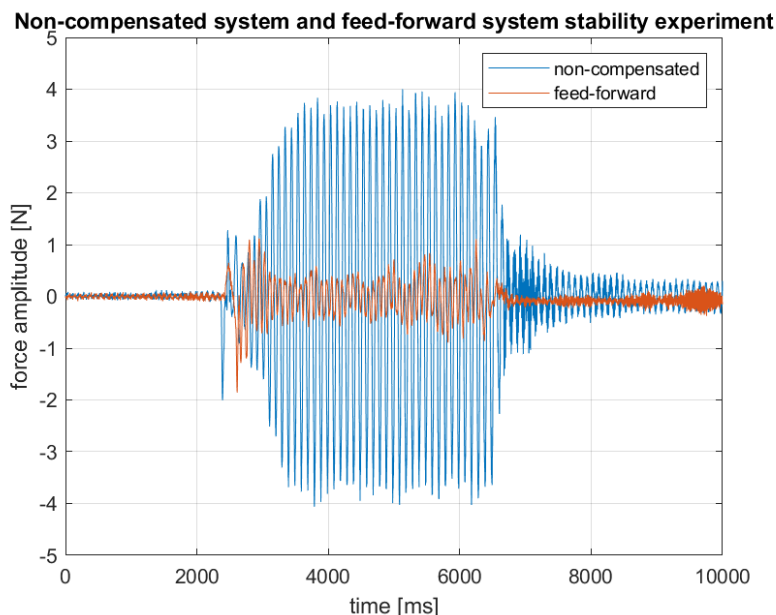
Figure 26. Non-compensated system and feed-forward system stability experiment with $M = 2\,\text{kg}$, $D = 1\,\text{Ns/m}$.

The result in Figure 26 shows that appending a feed-forward compensator to the system can improve the stability of the system. At $t = 0\,\text{s}$ to $t = 2.5\,\text{s}$, the machine is not in contact with humans, so both systems can remain stable, but at $t = 2.5\,\text{s}$ to $t = 6.5\,\text{s}$, where the human operator is in contact with the machine, it is clearly shown that a non-compensated system faces an aggressive oscillation, but on the other hand, the feed-forward system can reduce the oscillation by a significant amount, finally after $t = 6.5\,\text{s}$ where the human operator releases the contact, it shows that the feed-forward system can quickly eliminate the oscillation compared to a non-compensated system that still oscillates even though humans already release their grip.

6. FEEDBACK COMPENSATION

6.1. Design

A feedback compensator or feedback controller is a control system that will measure the output signal of the system and adjust the input signal to the system. Compared between the feed-forward and feedback compensators, both will improve the performance of the system, but the advantage of the feedback system is that it tends to have better robustness, which means it can maintain performance despite changes in the environment.

As shown in Figure 27, it is a feedback control system in this study, and we use acceleration as the feedback signal because directly measuring absolute structure displacement is not easy in a practice situation. Therefore, we use an accelerometer, which can easily be attached to the frame. The downside of an accelerometer is that it cannot accurately measure a low frequency, but it can be used in this study because we consider only the oscillation frequency range. In Figure 27, the block of s^2 represents the accelerometer to get the structure acceleration, a_f, from the structure displacement, x_f, and C_{fb} is a compensator transfer function.
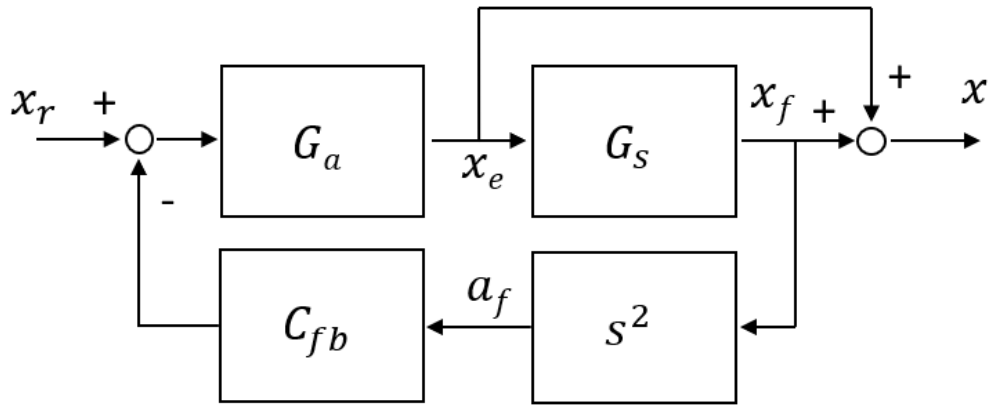
Figure 27. Feedback system block diagram.

To get better robustness to the change in structure characteristics, we need to make sensitivity small around the resonance frequency. The sensitivity of this system can be calculated using Equation (15).

$$S = \frac{\frac{\Delta G_{xxr}}{G_{xxr}}}{\frac{\Delta G_s}{G_s}} = \frac{\Delta G_{xxr}}{\Delta G_s} \frac{G_s}{G_{xxr}} \tag{15}$$

The experiment system with a feedback controller, which can be expressed in Figure 27, can be derived into Equation (16). To find the sensitivity of the system, we must derivate Equation G_{xxr} by the structure transfer function, as shown in Equation (17), G_s, and then multiply with $\frac{G_s}{G_{xxr}}$, as shown in Equation (18).

$$G_{xxr} = \frac{x}{x_r} = \frac{G_a(G_s + 1)}{G_a C_{fb} s^2 G_s + 1} \tag{16}$$

$$\frac{dG_{xxr}}{dG_s} = \frac{G_a(1 - G_a C_{fb} s^2)}{(G_a C_{fb} s^2 G_s + 1)^2} \tag{17}$$

$$S = \frac{dG_{xxr}}{dG_s} \frac{G_s}{G_{xxr}} = \frac{1 - G_a C_{fb} s^2}{1 + G_a C_{fb} s^2 G_s} \frac{G_s}{1 + G_s} \tag{18}$$

We need to design the compensator, C_{fb}, that makes the sensitivity small and also stabilizes the feedback system. We can use the Youla parameterization method[20], which is a design technique for the stable plant. Considering the feedback system shown in Figure 28, the Youla parameterization can be expressed in terms of a transfer function as Equation (19), where Q is the transfer function from r to u. Using this stable parameter, Q, all stabilizing compensators, C, are parameterized as Equation (20).
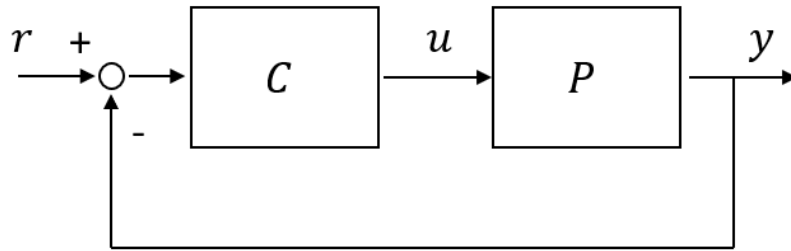
$$Q = \frac{C}{1 + PC} \tag{19}$$

Figure 28. Fundamental Youla block diagram.

$$C = \frac{Q}{1 - PQ} \tag{20}$$

In Equation (18), C_{fb} can be replaced from Equation (20), and the plant of the system, P, is equal to $G_a G_s s^2$, and we will get the result shown in Equation (21).

$$S = (1 - G_a s^2 Q(1 + G_s)) \frac{G_s}{1 + G_s} \tag{21}$$

Similarly, G_{xxr} can be expressed with the parameter Q as Equation (22).

$$G_{xxr} = G_a(1 + G_s)(1 - G_a G_s s^2 Q) \tag{22}$$

Equation (21) shows that if Q is expressed as Equation (23), the sensitivity of the system, S, will be 0. Furthermore, from Equation (22), G_{xxr} will be just G_a with the same Q; this means that the effect of the robot structure can be completely eliminated.

$$Q = \frac{1}{G_a s^2 (1 + G_s)} \tag{23}$$

But in reality, we know that G_a has an unstable zero that cause by dead time and also that $\frac{1}{s^2}$ is unstable itself. Therefore, the parameter Q in Equation (23) is not stable. So, G_a is divided into two parts, which consist of stable zero and unstable zero, as shown in Equation (24), and we only use G_{a0}, as shown in Equation (25), which is the stable zero part. The result of Q is shown in Equation (26).

$$G_a = G_{a0} * Pade\ approx. \tag{24}$$

$$G_{a0} = \frac{\omega_a^2}{s^2 + 2\zeta_a \omega_a s + \omega_a^2} \tag{25}$$

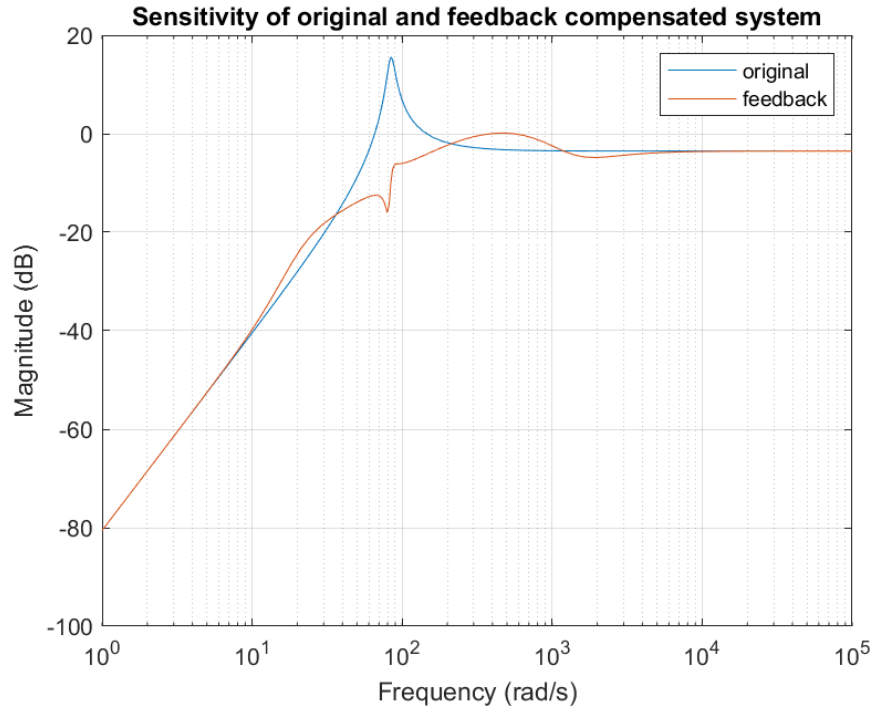$$Q = \frac{1}{G_{a0} s^2 (1 + G_s)} \tag{26}$$

Sensitivity of original and feedback compensated system

Figure 29. Sensitivity of original and feedback compensated system.

Because of unstable $\frac{1}{s^2}$, we must add at least a 2nd high-pass filter to make Q stable. But if we append a 2nd high-pass filter, the compensator will have some DC gain, so we use a 3rd high-pass filter to reject the offset or bias of the acceleration measurement. And also, we append a low-pass filter to reduce the noise effect and improve robust stability, resulting in Q that is shown in Equation (27).

$$
\begin{aligned}
Q &= \frac{1}{G_{a0}s^2(1+G_s)} \frac{s^3}{s^3 + 2\omega_1 s^2 + 2\omega_1^2 s + \omega_1^3} \frac{\omega_2}{s + \omega_2} \\
&= \frac{s\omega_2}{G_{a0}(1+G_s)(s^3 + 2\omega_1 s^2 + 2\omega_1^2 s + \omega_1^3)(s + \omega_2)}
\end{aligned}
\tag{27}
$$

Finally, we can replace Q in Equation (20) with Equation (27) to calculate the compensator transfer function, C_{fb}, as shown in Equation (28).

$$
C_{fb} = \frac{Q}{1 - G_a G_s s^2 Q} = \frac{s\omega_2}{G_{a0}(1+G_s)(s^3 + 2\omega_1 s^2 + 2\omega_1^2 s + \omega_1^3) - G_a G_s s^3 \omega_2}
\tag{28}
$$

Parameters ω_1, ω_2 are the cutoff frequencies of the high-pass filter and low-pass filter, respectively, and they must be selected so that the sensitivity of the system is reduced around the peak sensitivity of 80 rad/s, as shown in Figure 29. Here, the cutoff frequencies are considered across the peak frequency, and we select $\omega_1 = 22$ rad/s, $\omega_2 = 300$ rad/s, respectively.

In Figure 30, the Bode diagram shows the response of the overall robot transfer function, G_{xxr}, of the original system and feedback compensated system. It shows that the feedback compensation can reduce the effect
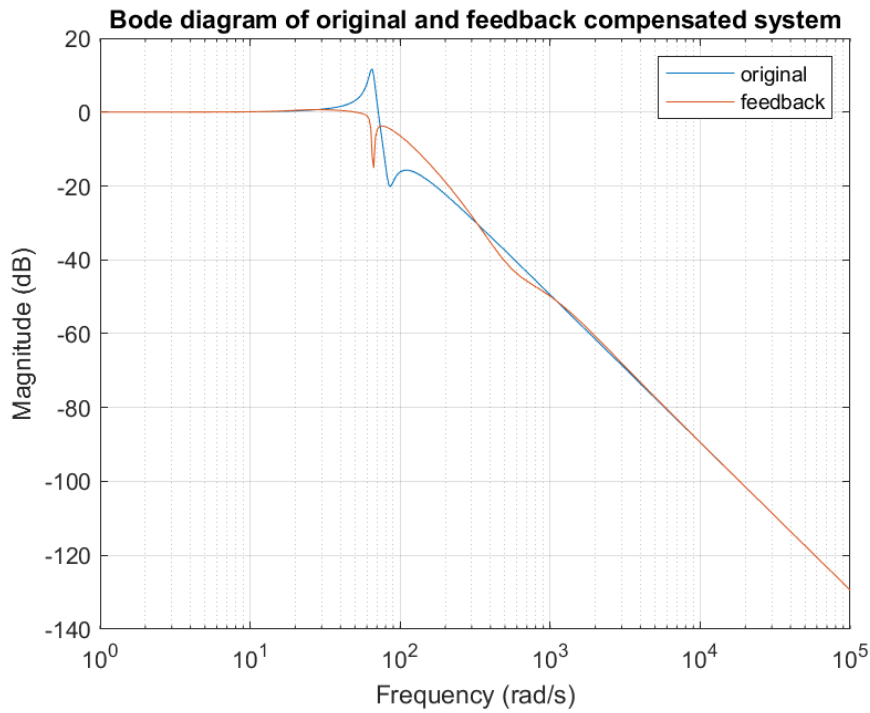
Bode diagram of original and feedback compensated system

Figure 30. Bode diagram of original and feedback compensated system.

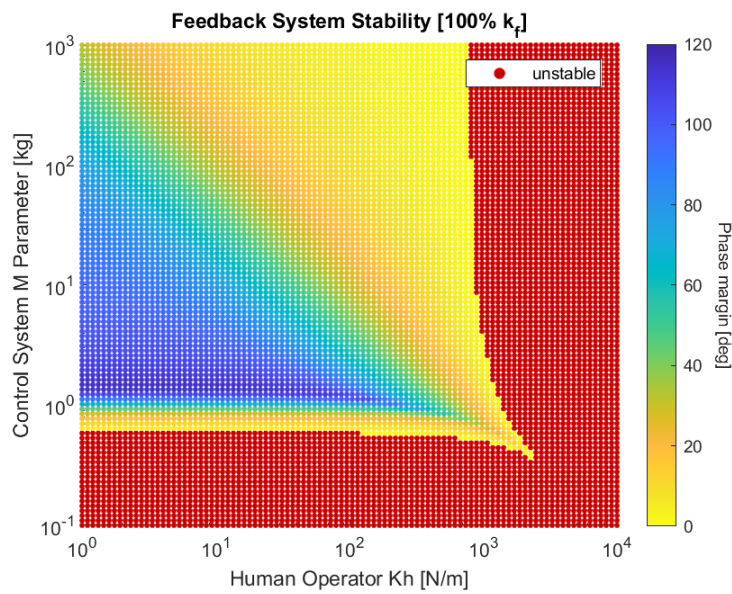**Feedback System Stability [100% k$_f$]**

Figure 31. Feedback system stability analysis with actual system structure stiffness at 100%.

of structure characteristics that occur in the original system. And also, because the sensitivity of the system in that region is reduced, the system can withstand the change in structure characteristics, which means the robustness of the system is increased.
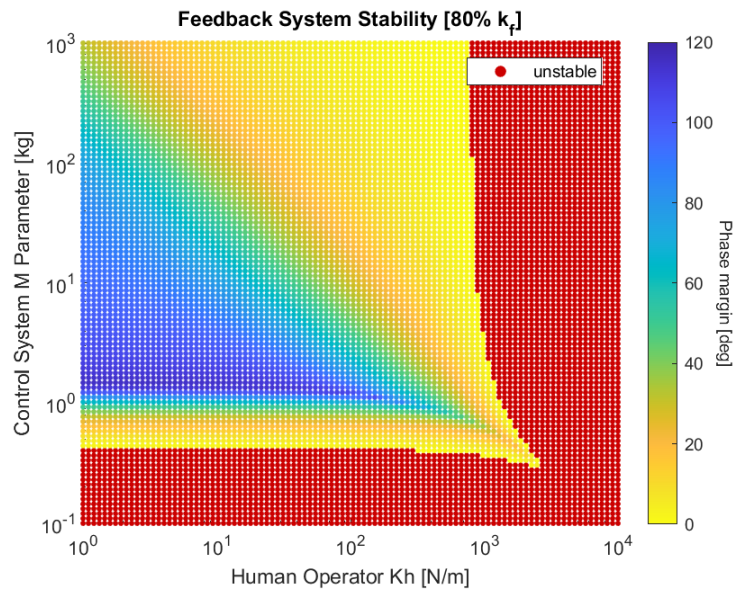
Feedback System Stability [80% k$_f$]

Figure 32. Feedback system stability analysis with actual system structure stiffness at 80%.

Feedback System Stability [120% k$_f$]
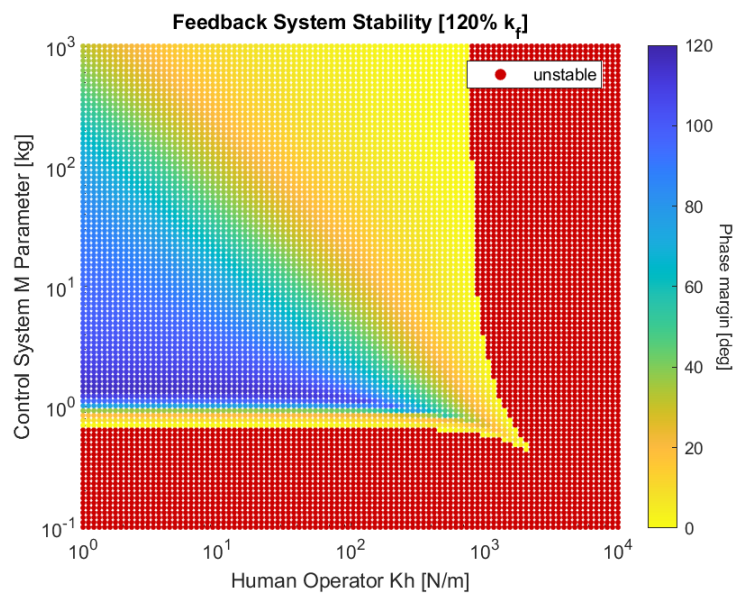
Figure 33. Feedback system stability analysis with actual system structure stiffness at 120%.

6.2. Simulation

The simulation is conducted using the same method as a feed-forward compensator simulation. Simulation with an actual system that has exactly the same stiffness as the measurement, as shown in Figure 31, the simulation with an actual system that has stiffness 20% less than the measurement, as shown in Figure 32, and a simulation with an actual system that has stiffness 20% greater than the measurement, as shown in Figure 33.

Figure 34. Stability region boundary comparison between a non-compensated system, a feed-forward system, and a feedback system at $100\% \, k_f$.
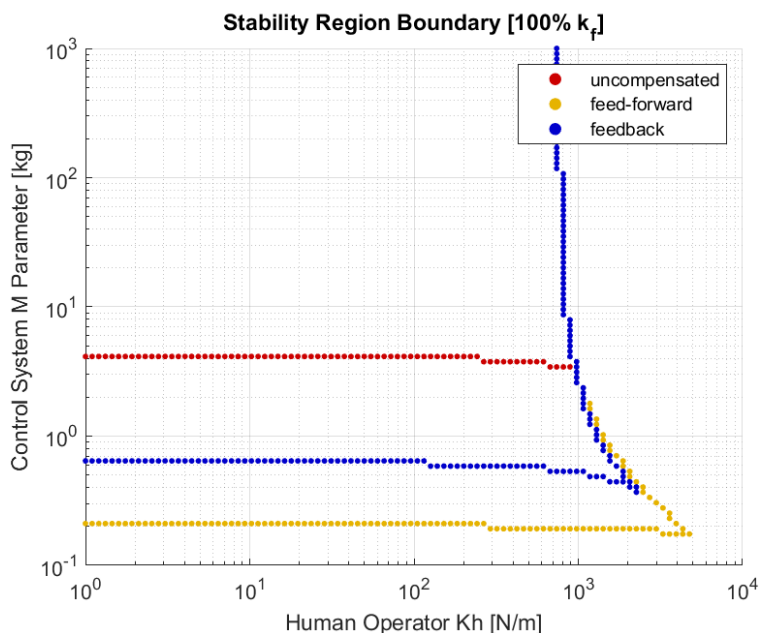
Figure 31 shows that the stability region is improved over a non-compensated system, but it is still smaller than the stability region achieved with feed-forward compensation, as shown in Figure 21. However, when the actual system structure stiffness decreases from measurement by 20%, the stability region slightly expands, as shown in Figure 32. On the other hand, as shown in Figure 33, the stability region still decreases when actual system stiffness increases from measurement by 20%, but it can remain stable compared to feed-forward in Figure 23.

In Figure 34, it is shown that when the compensator is perfectly canceling out structure characteristics in feed-forward compensation, it has an advantage in the stability region over the feedback system. But when the system is not perfectly compensated, as shown in Figure 35, it shows that the feedback system can remain stable with little change, but the stability region of the feed-forward system reduces significantly to the point that the feedback system has a greater stability region than the feed-forward system.

6.3. Experiment
In the experiment, we use the admittance model parameter as follows: $M = 2\,\text{kg}$, $D = 1\,\text{Ns/m}$, same as the previous experiment, so we can compare the result with feed-forward compensation.

From Figure 36, it is clear that a feedback compensator can greatly improve the stability of the system compared to a non-compensated system. However, Figure 36 also shows that the feedback system has low-frequency movement when a human operator is in contact with the machine, and it causes movement when the human operator attempts to make the end-effector remain in the same position. The damping parameter, D, of the admittance model should be larger than what we used in this experiment for precise movement operations[19]. We should consider changing the damping parameter according to the phase of the task; for example, during reaching movement, the damping, D, should be small, while for precise movements, larger damping, D, should be employed, which we will consider in future studies.

And when comparing feed-forward compensation with feedback compensation, as shown in Figure 37, feed-
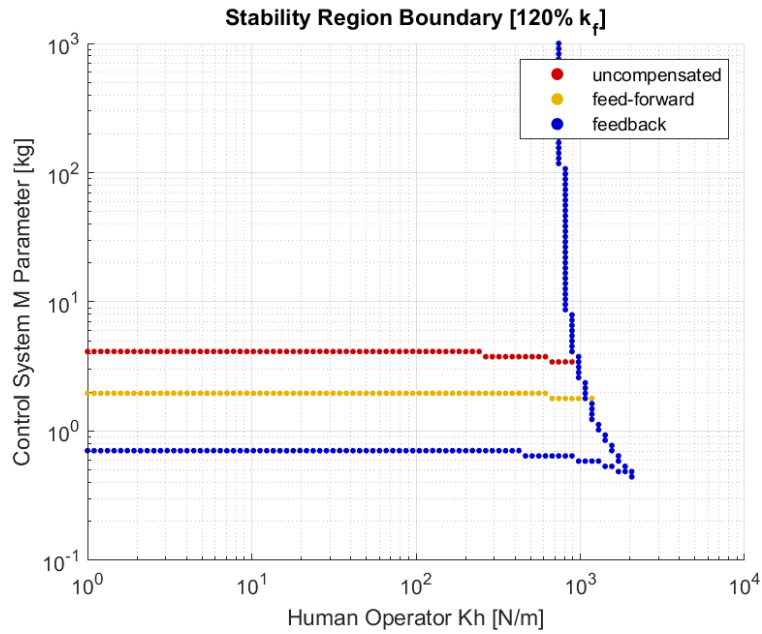
Figure 35. Stability region boundary comparison between a non-compensated system, a feed-forward system, and a feedback system at $120\% \, k_f$.
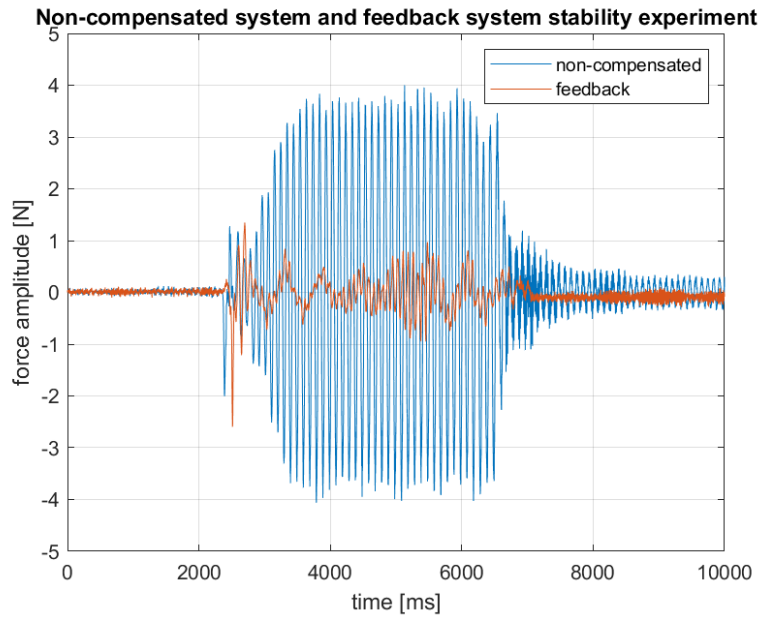
Figure 36. Non-compensated system and feedback system stability experiment with $M = 2\,\text{kg}$, $D = 1\,\text{Ns/m}$.

back compensation has a slight improvement in stability over feed-forward compensation in this condition, so we try another experiment with a smaller M parameter. The admittance model parameter is as follows: $M = 1\,\text{kg}$, $D = 1\,\text{Ns/m}$, which will make the feed-forward system unstable, but the feedback system can remain stable according to Figure 35, and the result is shown in Figure 38.

Feed-forward system and feedback system stability experiment

Figure 37. Feed-forward system and feedback system stability experiment with $M = 2\,\text{kg}$, $D = 1\,\text{Ns/m}$.

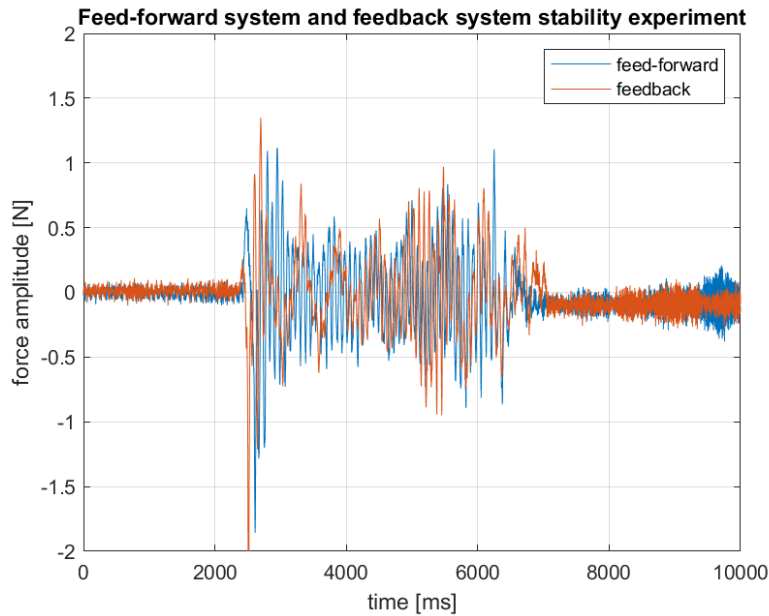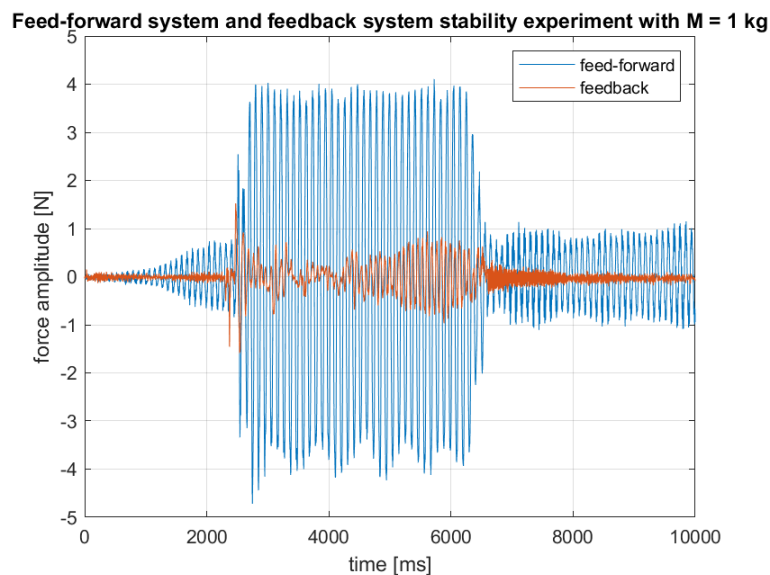**Feed-forward system and feedback system stability experiment with M = 1 kg**

Figure 38. Feed-forward system and feedback system stability experiment $M = 1\,\text{kg}$, $D = 1\,\text{Ns/m}$.

Figure 38 shows that in a feed-forward system, it cannot remain stable even when a human operator is not in contact with it, and it starts to aggressively oscillate when a human is in contact at $t = 2.5\,\text{s}$ to $t = 6.5\,\text{s}$. On the other hand, a feedback system can remain stable the whole time with a little oscillation when a human operator is in contact with them.

Figure 37 and Figure 38 show that when we change parameter M in the admittance model, the feedback-compensated system can remain stable with operator interaction force within ±1N. Low-frequency force in the graph comes from the instability of the human-machine system, which is caused by the low damping

parameter in the admittance model, D. However, the high-frequency oscillation force is greatly reduced compared with a feed-forward system, which means the influence of insufficient structure stiffness is compensated with feedback.

7. CONCLUSION

In this study, we know that the human-machine system will face an unstable situation when a human operator is in contact with the machine when the stiffness of the structure is not high enough. Therefore, we have two methods of adding a compensator to the system that helps improve the stability region of the human-machine system, so we can use a lighter weight in the admittance model, which means the operator can work in a lighter load environment.

The first one is a feed-forward compensator, which uses the inverse of the structure transfer function to cancel out structure characteristics that cause oscillations. The simulation section shows that the stability region is greatly improved over an uncompensated system, and we can use a lower M parameter in the admittance model. Even though the actual structure parameter is different from the measurement, the stability region is smaller than the ideal one, but it still shows an improvement over an uncompensated system. To confirm our simulation, we conduct an experiment with the M parameter in the admittance system equal to 2 kg. The result is as expected, an uncompensated system will oscillate when a human operator is in contact, but a feed-forward system can remain stable. Therefore, this experiment can confirm that this method of compensation can improve the stable operation range of the system.

With feed-forward compensation, the stability region is greatly reduced by the difference between the measurement and the actual parameter. So, we tried a feedback compensator with an accelerometer, which is another method to compensate for structure characteristics. Although in simulation, it shows that the stability region is not improved from an uncompensated system as much a feed-forward system. However, we consider conditions when a structure parameter is different from what we measure. It shows that the feedback system is greatly improved over the feed-forward system, and it can remain stable when actual structure parameters change. From the experiment, it is also confirmed that the feedback system has an advantage over the feed-forward system, with $M = 1$ kg feedback system can remain stable, but the feed-forward system is unstable. This indicates that simple feedback using accelerometers can compensate for the insufficient stiffness of the robot structure and greatly enhance the stability of the human-machine system.

Furthermore, we plan to refine the admittance model design because we know that the stability of the system also depends on human interaction, which causes differences in each movement due to changes in human impedance, so we will use a dynamic variable in the admittance model. It will be changed according to human movement and task so the operator can move the object with a light force during a traveling task and can perform a high-precision task when needed. The feedback compensation studied in this study should increase the range of variation in the admittance model.

DECLARATIONS

Authors' contributions
Conducted the experiment, simulation, data acquisition, and data analysis: Songthumjitti N

Conceived and designed the study: Inaba T

Interpreted the results: Songthumjitti N, Inaba T

Availability of data and materials
Not applicable.

Financial support and sponsorship

None.

Conflicts of interest

All authors declared that there are no conflicts of interest.

Ethical approval and consent to participate

Not applicable.

Consent for publication

Not applicable.

Copyright

© The Author(s) 2023.

REFERENCES

1. Villani V, Pini F, Leali F, Secchi C. Survey on human-robot collaboration in industrial settings: safety, intuitive interfaces and applications. *Mechatronics* 2018;55:248-66. DOI

2. Matheson E, Minto R, Zampieri EGG, Faccio M, Rosati G. Human-robot collaboration in manufacturing applications: a review. *Robotics* 2019;8:100. DOI

3. Hentout A, Aouache M, Maoudj A, Akli I. Human-robot interaction in industrial collaborative robotics: a literature review of the decade 2008 - 2017. *Advanced Robotics* 2019;33:764-99. DOI

4. Krüger J, Lien T, Verl A. Cooperation of human and machines in assembly lines. *CIRP Annals* 2009;58:628-46. DOI

5. Keemink AQ, van der Kooij H, Stienen AH. Admittance control for physical human-robot interaction. *Int J Rob Res* 2018;37:1421-44. DOI

6. Lawrence DA. Impedance control stability properties in common implementations. In: Proceedings. 1988 IEEE International Conference on Robotics and Automation; 1988. p.1185-90. DOI

7. Tsumugiwa T, Yokogawa R, Yoshida K. Stability analysis for impedance control of robot for human-robot cooperative task system. In: Proceedings of 2004 IEEE/RSJ International Conference on Intelligent Robots and Systems (IROS); 2004. p. 3883-8. DOI

8. Calanca A, Muradore R, Fiorini P. A review of algorithms for compliant control of stiff and fixed-compliance robots. *IEEE/ASME Trans Mechatron* 2016;21:613-24. DOI

9. Tsumugiwa T, Fuchikami Y, Kamiyoshi A, Yokogawa R, Yoshida K. Stability analysis for impedance control of robot in human-robot cooperative task system. *J Adv Mech Des Systs Manufacturing* 2007;1:113-21. DOI

10. Sharkawy A, Koustoumpardis PN. Human-robot interaction: a review and analysis on variable admittance control, safety, and perspectives. *Machines* 2022;10:591. DOI

11. Kang G, Oh HS, Seo JK, Kim U, Choi HR. Variable admittance control of robot manipulators based on human intention. *IEEE/ASME Trans Mechatron* 2019;24:1023-32. DOI

12. Lecours A, Mayer-St-Onge B, Gosselin C. Variable admittance control of a four-degree-of-freedom intelligent assist device. In:2012 IEEE International Conference on Robotics and Automation; 2012. p. 3903-8 DOI

13. Dimeas F. Online stability in human-robot cooperation with admittance control. *IEEE Trans Haptics* 2016;9:267-78. DOI

14. Ferraguti F, Talignani Landi C, Sabattini L, Bonfè M, Fantuzzi C, Secchi C. A variable admittance control strategy for stable physical human - robot interaction. *Int J Rob Res* 2019;38:747-65. DOI

15. Müller F, Janetzky J, Behrnd U, Jäkel J, Thomas U. User force-dependent variable impedance control in human-robot interaction. In: 2018 IEEE 14th International Conference on Automation Science and Engineering (CASE);2018. p. 1328-35. DOI

16. Buerger SP, Hogan N. Complementary stability and loop shaping for improved human-robot interaction. *IEEE Trans Robot* 2007;23:232-44. DOI

17. Narawich SONGTHUMJITTI, Takeshi INABA, Modeling and stability analysis of an admittance-controlled cartesian robot considering physical interaction with humans. In: The 23rd Conference of The System Integration Division, The Society of Instrument and Control Engineering, 3P3-E18 (2022)

18. Inaba T, Shu U. Control of power assist system for easy positioning consideration to maneuverability depending on task direction and operator's posture. *IEEJ Trans EIS* 2014;134:1130-7. DOI

19. Inaba T, Matsuo Y. Loop-shaping characteristics of a human operator in a force reflective manual control system. In: Systems, Man, and Cybernetics, 1997. Computational Cybernetics and Simulation, 1997 IEEE International Conference on. IEEE, 1995. DOI

20. Keviczky L, Bars R, Hetthéssy J, Bányász C. Control engineering. *Springer Singapore* (2019). DOI